

HALL-PETCH DEPENDENCE OF J-FRACTURE TOUGHNESS PARAMETERS FOR A RPV STEEL - PART I: ANNEALED MICROSTRUCTURES

José Ricardo Tarpani

Materials, Aeronautical and Automotive Engineering Department, Engineering School of São Carlos – University of São Paulo – Brazil
jrpan@sc.usp.br

Waldek Wladimir Bose Filho

Materials, Aeronautical and Automotive Engineering Department, Engineering School of São Carlos – University of São Paulo – Brazil
waldek@sc.usp.br

Dirceu Spinelli

Materials, Aeronautical and Automotive Engineering Department, Engineering School of São Carlos – University of São Paulo – Brazil
dspinell@sc.usp.br

Abstract. The elastic-plastic fracture toughness and crack extension behavior under quasi-static loading regime of several microstructures of a reactor pressure vessel steel were assessed on the basis of microstructural parameters. J-integral fracture toughness testing were conducted at 300° via the unloading elastic compliance technique. Miniaturized compact test specimens, 0.2T and 0.4 C(T) (5 and 10mm-thick, respectively), were machined from thick forged plates (T/4 position, T-L orientation) of the microalloyed steel in the as-received and the several thermally embrittled conditions. Through a simple rule of mixture typically applied for composite materials, it has been discovered that the equivalent grain size of dual-phase (ferrite/bainite) annealed microstructures controls their J-fracture toughness properties. It has also been concluded that J-fracture toughness parameters correlate to the equivalent grain size by means of Hall-Petch relationship. These conclusions have been shown to hold regardless the J-R curve fitting method adopted, namely the widely used power-law, the here proposed logarithmic fit and the old-dated linear fit method.

Keywords. fracture toughness, Hall-Petch relationship, J-R curve, RPV steel, thermal embrittlement.

1. Introduction

In the last decade, Onizawa et al (1997) and de Diego et al (1998) have successfully simulated the irradiation damage effects on the mechanical behavior of metals by means of heat and thermo-mechanical treatments, respectively. However, none of these studies have made explicit references to the effect of microstructural variables (e.g. grain size and phase percentage) on the mechanical performance of the so-embrittled metallic alloys.

In this work, a nuclear grade steel was submitted to annealing heat treatments in order to evaluate the microstructural parameters controlling the fracture mechanisms acting on the different grades of thermal embrittlement levels. Additional microstructures obtained from quenching and tempering heat treatments will be further presented in Part II by Tarpani et al (2003).

2. Base material

A typical reactor pressure vessel (RPV) material for the nuclear industry, ASTM A508-3A steel (chemistry in Tab. 1), was utilized for this study.

Figure (1a) shows schematic drawing of its original heat treatment, and Fig. (1b) pictures the resultant microstructure (denoted A), named granular or globular bainite in the Bramfitt & Speer's nomenclature (1990). This single-phase microstructure exhibits a mean grain diameter of 19 μm (8.5 ASTM grain size number).

Table 1 - Chemical composition determined for the A508 nuclear grade steel (wt%).

C	Si	Mn	Ni	Mo	Cr	Al	P	S
0.19	0.24	1.30	0.72	0.51	0.03	0.012	0.007	0.009

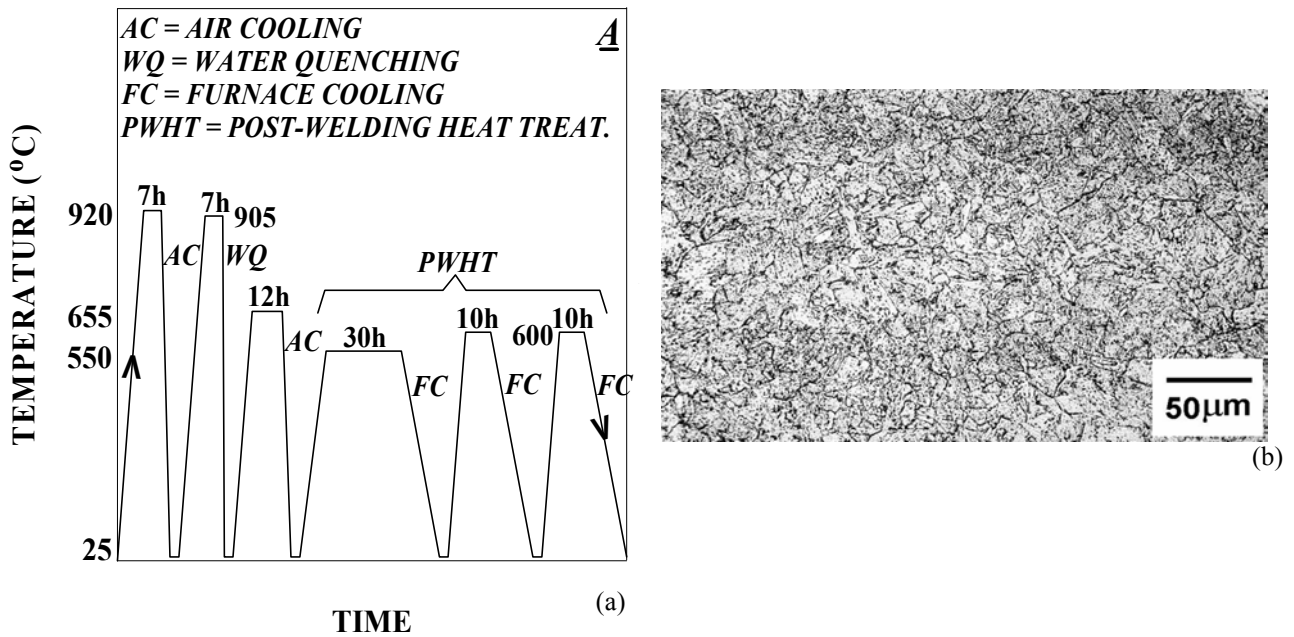


Figure 1. (a) Schematic drawing of fabrication thermal cycle of the A508-3A RPV steel; (b) As-received microstructure (A) exhibiting granular or globular bainite. Nital 2% etch.

3. Experimental and analytical procedures

3.1 Annealing thermal cycles

Figure (2a) shows schematic drawings of the seven embrittling heat treatments, named from B to H, individually applied to the A508 steel.

3.2 Conventional mechanical properties and J-fracture toughness tests

Hardness measurements at ambient temperature and tensile tests at 300°C, were carried out for the base and thermally embrittled materials.

Fracture mechanics J-R curve testing were performed according to ASTM standard (1997) via the unloading elastic compliance technique under clip-gage-controlling elastic unloading in a computer-controlled closed-loop servo hydraulic machine. For this purpose, miniaturized 5 mm and 10 mm-thick compact tensile specimens were machined from the one-quarter-thickness position of the as-received and thermally embrittled forged plates in T-L orientation. They were pre-cracked to a nominal 0.5 a_0/W ratio, side-grooved (SG) to 20% and 33% (for a maximum plastic constraint, Zhang & Shi, 1992) of their gross-thickness, and tested at 300°C, a typical operational RPV temperature, under a cross-head speed of 0.3 mm/min. Once traced the J-R curves (see Eqs. 1-3), the ASTM standard (1997) J initiation value, J_i , and the Paris & Johnson's (1983) J_{50} parameter, which is commonly used to predict ductile tearing instability of pressurized flawed components were determined. A third fracture mechanics index, as proposed by Hackett, & Joyce (1992), mathematically expressed by $dJ_D/d\Delta a_{(1mm)}$, namely, the rate of increase on the resistance to crack growth at 1 mm of crack propagation, was also derived from J-R curves. Power-law (Eq. 1), logarithmic (Eq. 2) and linear (Eq. 3) fits simultaneously applied to the $J-\Delta a$ data points located within well-defined limits of validity of the deformation-J (J_D) concept as established in the ASTM standard (1997), are as follows:

$$J = b \cdot (\Delta a)^c \quad (1)$$

$$J = d \cdot \ln \Delta a + e \quad (2)$$

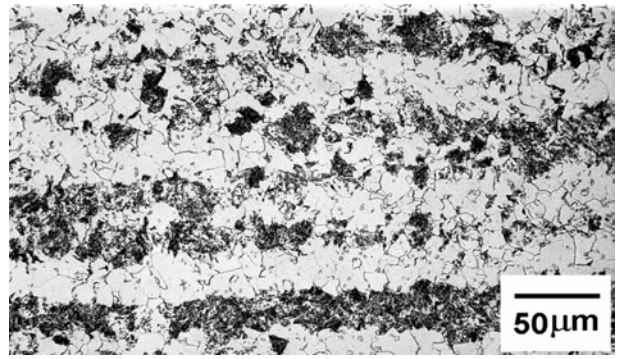
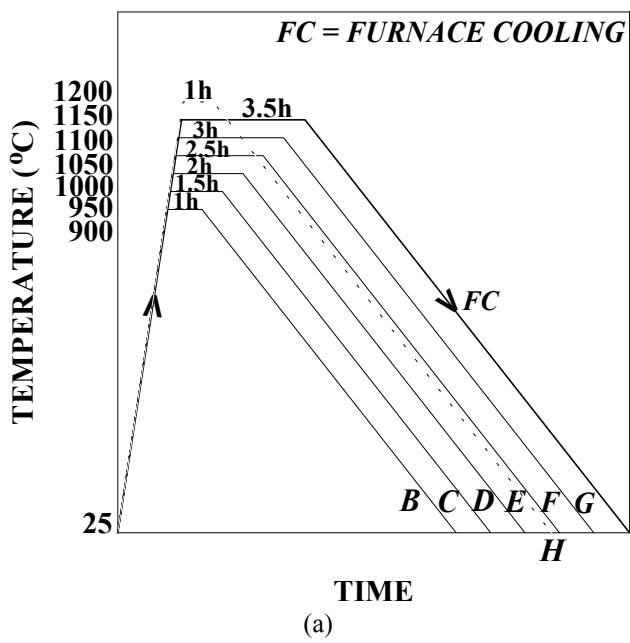
$$J = f \cdot \Delta a + g \quad (3)$$

where b, c, d, e, f and g are fitting constants.

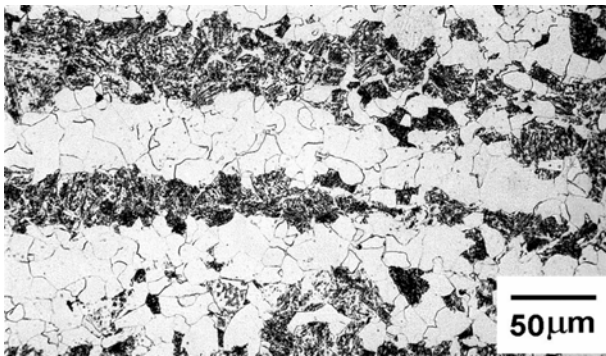
4. Results and discussion

4.1 Microstructural characterization

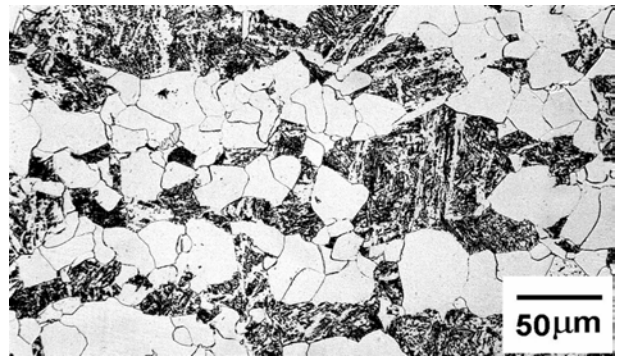
Figures (2b-h) depict microstructures of the evaluated materials. They comprise essentially of a mixture of nearly equiaxial grains of ferrite and globular low carbon bainite. Mean grain diameters and phase percentages were determined for the thermally embrittled microstructures by using a computerized image analyzer.



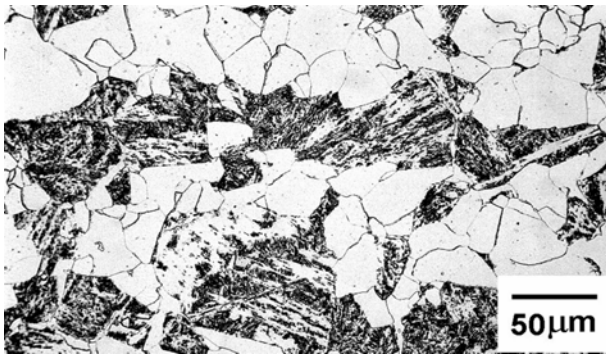
(b)



(c)



(d)



(e)



(f)



(g)



(h)

Figure 2. (a) Schematic drawing of annealing routes aimed at producing thermally embrittled microstructures from original A508 steel (A). Light micrographs of embrittled microstructures B (b), C (c), D (d), E (e), F (f), G (g) and H (h). Etchant: Nital 2%.

Table (2) shows that, as expected, both ferrite and bainite grains size enlarges with the annealing severity (B→H), and a quite outstanding acceleration on bainite grain size is noticed for the microstructures G and H. It can be seen that milder annealing cycles generate both phases in a fixed proportion, of about 1:1, but in the latter microstructures there is far more bainite than ferrite.

Higher austenitization temperatures, providing larger prior austenite grain size in the microstructures G and H, gave rise to higher hardenabilities, and accompanying microstructural refinement, thus preventing the pro-eutectoid ferrite phase from being nucleated during furnace cooling. Accordingly, a competition between grain size and microstructural refinement, the latter denoted by the acicularization of the bainite phase, is likely to occur due to increasing austenitization temperature.

Banding decreases as the severity of the annealing heat treatment is increased, i.e. along with the bainite refinement and grain growth. The thermal conditions leading to the loss of banding in microstructures G and H, gave rise to a very unusual arrangement between bainite and ferrite phases. Very large grains of the former are completely surrounded by a network of relatively quite small grains of the latter, which exhibits a very broad grain size distribution.

Table 2 - Microstructural parameters of materials. ASTM grain size number is given in brackets.

Annealing Route	D _{ferrite} (μm)	D _{bainite} (μm)	% Phase ferrite / bainite
B	20 (8.3)	19 (8.5)	48 / 52
C	30 (7.2)	26 (7.6)	49 / 51
D	39 (6.4)	50 (5.7)	50 / 50
E	47 (5.9)	56 (5.4)	50 / 50
F	50 (5.7)	64 (5.0)	51 / 49
G	55 (5.4)	475 (0)	19 / 81
H	61 (5.1)	817 (00)	11 / 89

4.2 Hardness and tensile properties

Table (3) lists typical conventional mechanical properties of tested materials.

Table 3 - Hardness and tensile properties of as-received and annealed materials tested.

Material	Brinell (100 kgf)	S _Y (MPa)	S _U (MPa)	EL (%)	RA (%)
A	175	400	555	11	77
B	170	360	620	17	71
C	167	345	610	16	63
D	168	370	620	12	54
E	169	375	625	12	49
F	192	450	675	11	39
G	198	470	685	05	31
H	208	490	665	05	28

D₀=4mm; L₀/D₀=10

As will be seen later in this text, the reduction in area results provided in Table 3 clearly indicate the impairment of the fracture toughness of the materials tested, as a consequence of higher temperatures and longer residence times applied during the annealing heat treatments.

As seen in Tab. (2), RA also exhibits an inverse correlation to the granulometry of both phases present in all the annealing products, resembling the so-called Hall-Petch relationship (Hall, 1951 & Petch, 1953), where the mechanical property vary inversely to the root squared grain size.

A representative parameter for the composed granulometry of the annealed products, that is, an equivalent grain size, EGS, can be established on the basis of the rule of mixture, typically applied to composite materials:

$$EGS = ((D_{ferrite}) \cdot (\% Ferrite) + (D_{bainite}) \cdot (\% Bainite))/100 \quad (4)$$

where the ferrite and bainite grain sizes, respectively D_{ferrite} and D_{bainite}, are furnished in Tab. (2) along with both phase percentages.

Figure (3) displays the relationship between RA and EGS, where good data correlation is achieved as indicated by the coefficient R. A Hall-Petch relationship correlates RA to EGS values as follows:

$$RA = h + i \cdot EGS^{-0.5} \quad (5)$$

where h and i are fitting constants.

This relationship indicates that RA is rather grain-size driven than controlled by the concurrent bainite refinement.

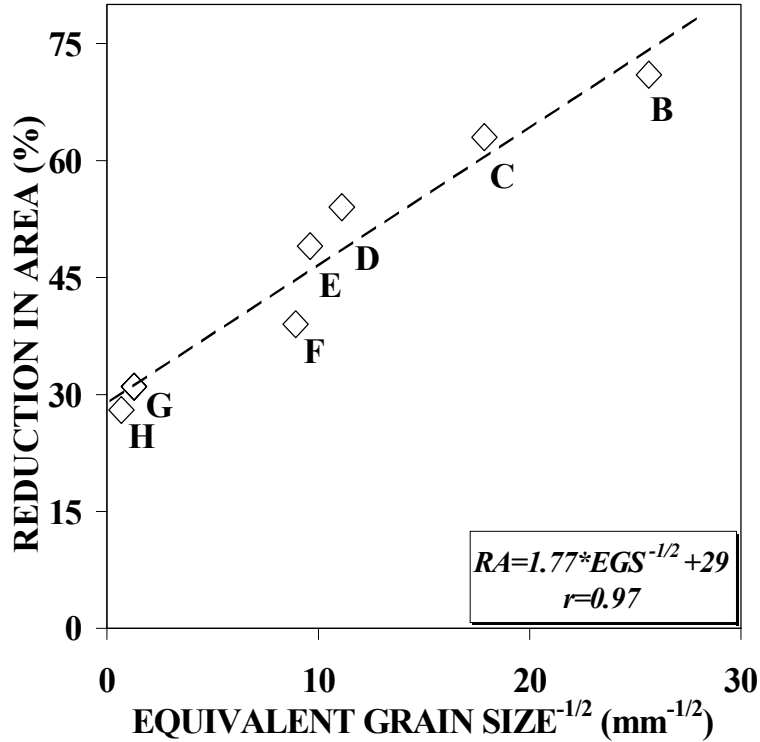


Figure 3. Hall-Petch dependence of RA on EGS, according to Eq. (5).

4.3 J-R curves and fracture toughness parameters

Figure (4) presents typical $J-\Delta a$ data points determined for all thermal conditions of the A508-3A steel. Extensive ductile crack growth, typically in the range 2-4 mm, is verified. The effect of deeper side-grooving level (33%SG, in Fig. 4b, against 20% SG, in Fig. 4a) in steeping down the J-R curves is clearly noticed as a result of higher plastic constraint.

In general, it can be observed that the rank established for RA, in terms of EGS (see Fig. 3), is faithfully obeyed for the J-R curves positioning, signaling that EGS also controls the ductile crack growth resistance of the materials tested.

The unexpected slight better performance of microstructure D over C, on the basis of EGS concept, is possibly explained by an eventual slighter major role played by bainite refinement over the equivalent grain size.

Concerning microstructure H, the sigmoidal arrangement of $J-\Delta a$ data is probably due to the development of cumulative fatigue damage during the pre-cracking procedure. Fatigue micro-cracking spread into the fracture process zone at the crack tip, thus embrittling the material and consequently leading to a very poor initial resistance to monotonic crack propagation on J-R curve testing.

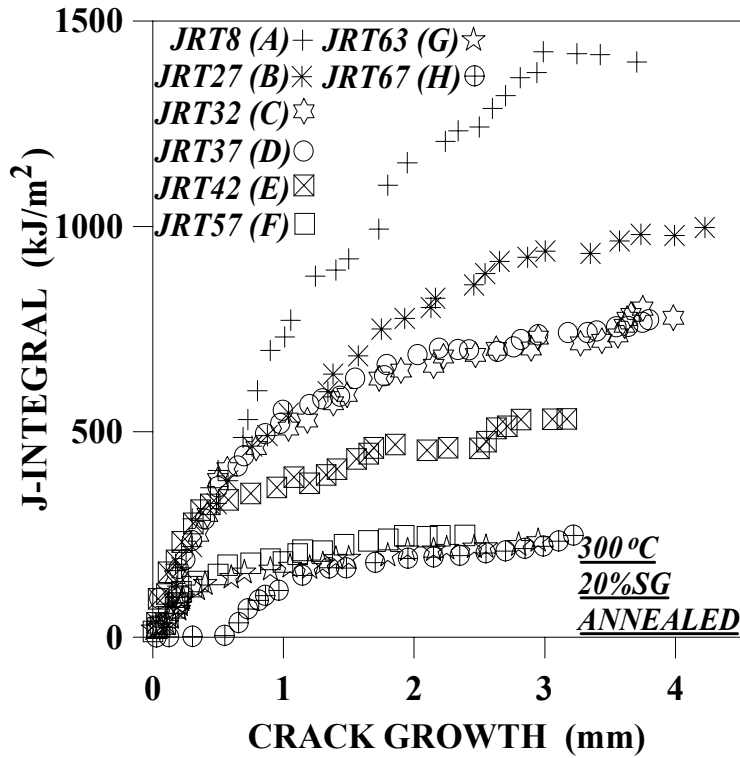
Besides the conservatism of J-R curves derived from deeper side-grooved test specimens, Fig. (4b) displays a J-specimen size dependence for microstructure G. A thinner testpiece originated a less conservative J-R curve due to the loss of plastic constraint, i.e. triaxial stress state relaxation along crack leading edge.

In Fig. (5), the dependence of J-parameters, namely J_i , J_{50} and $dJ_D/d\Delta a_{(1mm)}$, on EGS is shown for the three distinct J-R (i.e. $J-\Delta a$) data fitting methods applied, according to a Hall-Petch relationship given by:

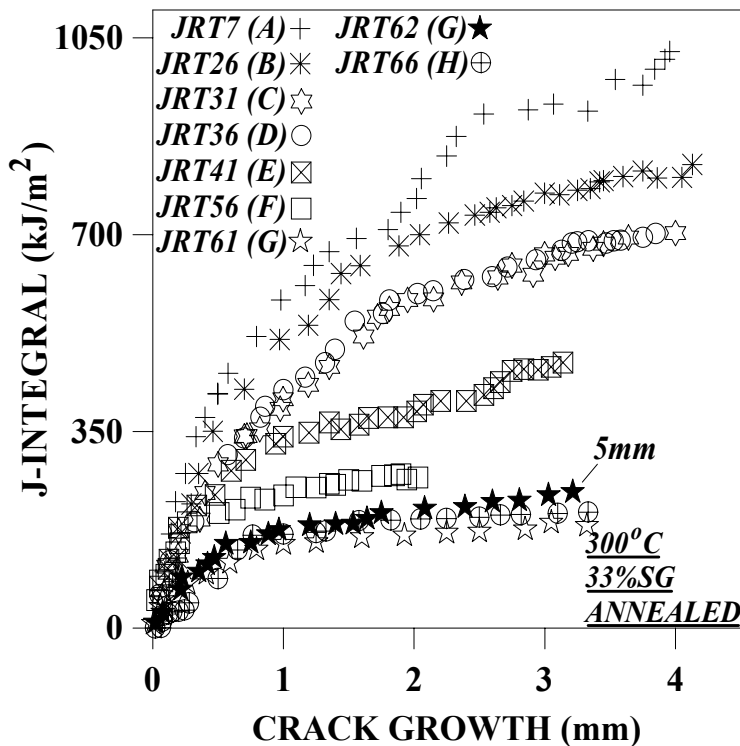
$$J = j + k \cdot EGS^{-0.5} \quad (6)$$

where j and k are fitting constants.

Figure (5) unequivocally depicts the conservative aspect of the logarithmic fit of J - Δa data points in generating lower J_i and J_{50} values, as compared to power-law and mainly linear data fitting. Observe that this conclusion does not apply to the $dJ_D/d\Delta a_{(1mm)}$ criterion. In fact, an inverted behavior is noticed regarding the latter fracture-toughness parameter. The same figure confirms earlier predictions that more conservative J -criteria are determined by testing deeper side-grooved test specimens (Fig. 4). As previously mentioned (see Fig. 4b), a slight specimen-size effect is also observed in Fig. (5), when thinner J -testpiece of microstructure G conducted to less conservative J -criteria results. Note that this effect is almost imperceptible for the $dJ_D/d\Delta a_{(1mm)}$ criterion.



(a)



(b)

Figure 4. Typical J - Δa curves of the tested materials. (a) 20% SG; (b) 33% SG compact specimens. Testpieces are 10 mm-thick unless otherwise indicated.

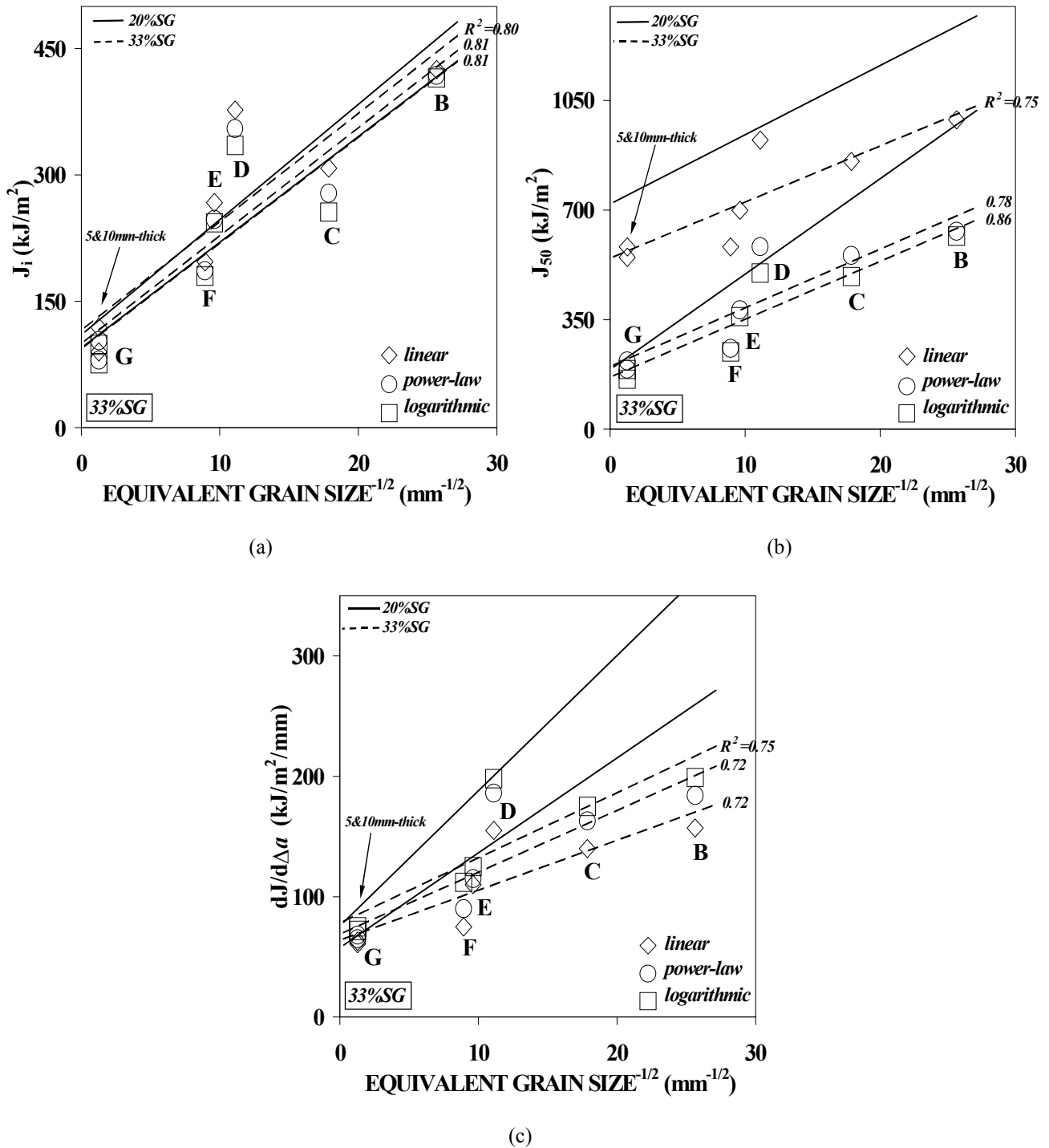


Figure 5. Hall-Petch dependence of J-parameters on EGS, according to Eq. (6): (a) Crack initiation J_i ; (b) Crack instability J_{50} , and (c) Rate of increase on cracking resistance $dJ/d\Delta a$. Testpieces are 10mm-thick unless otherwise indicated.

5. Concluding remarks

The elastic-plastic fracture toughness and crack extension behavior under quasi-static loading regime of the as-received and several thermally embrittled conditions of a nuclear reactor pressure vessel (RPV) steel were assessed on the basis of microstructural parameters.

By using a simple rule of mixture it has been found that the equivalent grain size (EGS) concept of dual-phase annealed microstructures is the chief fracture properties controlling factor, which depends on EGS in a Hall-Petch manner.

The procedure was based on the relative percentage of the phases present in the thermally embrittled microstructures, therefore similar to that proposed for the inference of mechanical properties of composite materials.

These conclusions have been shown to hold regardless the adopted J-R curve fitting method.

6. Acknowledgment

The authors gratefully acknowledge the financial support provided by FAPESP (contract 97-05652/1).

7. References

- Anonymous, 1997, "Standard Test Method for Measurement of Fracture Toughness", Designation ASTM E-1820, Annual Book of ASTM Standards, in CD.
- Bramfitt, L.B. and Speer, J.G., 1990, "A Perspective on the Morphology of Bainite", Metall. Trans., Vol.21A, pp. 817-829.
- de Diego, G., Castaño, Ma.L. and Hernández, M., 1998, "Simulación del Efecto de la Irradiación Mediante el Trabajado en Frío y los Tratamientos Térmicos en los Aceros Inoxidables Austeníticos", Rev. Metall. (in Spanish), Vol.34, pp. 407-420.
- Hackett, E.M. and Joyce, J.A., 1992, "Use of J-R Curves in Assessing the Fracture Behavior of Low Upper Shelf Toughness Materials", Nucl. Engng Des., Vol.134, pp. 217-226.
- Hall, E.O., 1951, "The Deformation and Ageing of Mild Steel, Proc. Phys. Soc. B., Vol.64, pp. 747-753.
- Onizawa, K., Fukai, K., Nishiyama, Y., Suzuki, M., Kaihara, S. and Nakamura, T., 1997, "Development of a Reconstitution Technique for Charpy Impact Specimens by Surface-Activated Joining for Reactor Pressure Vessel Surveillance", Int. J. Pressure Vessels Piping, Vol.70, pp. 201-207.
- Paris, P.C. and Johnson, R.E., 1983, "A Method of Application of Elastic-Plastic Fracture Mechanics to Nuclear Vessels Analysis", ASTM STP (Special Technical Publication) 803, Vol.2, pp. 05-40.
- Petch, N.J., 1953, "The Cleavage Strength of Polycrystals, J. Iron Steel Inst., Vol.174, pp 25-28.
- Tarpani, J.R., Bose Filho, W.W. and Spinelli, D., 2003, "Hall-Petch Dependence of J-Fracture Toughness Parameters for a RPV Steel - Part II: Quenched and Tempered Microstructures". Proceedings of the 24th Brazilian Congress of Mechanical Engineering, São Paulo, Brazil.
- Zhang, X.P. and Shi, Y.W., 1992, "Constraint of Side-Groove and Its Influence on Fracture Toughness Parameter in Charpy-Size Specimens, Engng Fract. Mech., v.43, pp. 863-867.